Advances in Applied Mathematics and Mechanics
Adv. Appl. Math. Mech., Vol. **8**, No. 5, pp. 795-809

DOI: 10.4208/aamm.2015.m1083
October 2016

Aeroacoustic Simulations Using Compressible Lattice Boltzmann Method

Kai Li and Chengwen Zhong*

National Key Laboratory of Science and Technology on Aerodynamic Design and Research, Northwestern Polytechnical University, Xi'an 710072, China

Received 2 May 2015; Accepted (in revised version) 11 August 2015

Abstract. This paper presents a lattice Boltzmann (LB) method based study aimed at numerical simulation of aeroacoustic phenomenon in flows around a symmetric obstacle. To simulate the compressible flow accurately, a potential energy double-distribution-function (DDF) lattice Boltzmann method is used over the entire computational domain from the near to far fields. The buffer zone and absorbing boundary condition is employed to eliminate the non-physical reflecting. Through the direct numerical simulation, the flow around a circular cylinder at $Re = 150$, $M = 0.2$ and the flow around a NACA0012 airfoil at $Re = 10000$, $M = 0.8$, $\alpha = 0^\circ$ are investigated. The generation and propagation of the sound produced by the vortex shedding are reappeared clearly. The obtained results increase our understanding of the characteristic features of the aeroacoustic sound.

AMS subject classifications: 65M10, 78A48

Key words: Lattice Boltzmann method, compressible flow, double-distribution-function, direct numerical simulation, aeroacoustics.

1 Introduction

Computational aeroacoustics (CAA) is a very useful way to predict the generation of noise through numerical methods. At present, there are two major categories of CAA [1, 2]. The first one is the hybrid method in which the flow field is simulated first to find the acoustic source strength of the flow and then the acoustic field is calculated in the surrounding domain. The hybrid method had a weakness that the feedback effects of sound to flow is not considered. The direct method in which the acoustic field is a natural part of the flow field has no such problem. Compared with the hybrid method, computational

*Corresponding author.
Email: lik@mail.nwpu.edu.cn (K. Li), zhongcw@nwpu.edu.cn (C. W. Zhong)

 ©2016 Global Science Press

https://doi.org/10.4208/aamm.2015.m1083 Published online by Cambridge University Press

cost of the direct method is high to provide the details of sound generating mechanisms. With the development of the computer technology, the direct method has become popular [3–5].

Lattice Boltzmann (LB) method is now a very powerful tool of computational fluid dynamics (CFD). Different with the traditional Navier-Stokes equations based CFD methods, LB method is a mesoscopic approach based on kinetic theory of fluids and can bring more information of complex flow behavior [6, 7]. After the introduction of the Bhatnagar-Gross-Krook (BGK) model [8], LB method also has simpler mathematical expressions. Through the Chapman-Enskog expansion, Navier-Stokes equations can be derived from LB model [9]. Thus many scholars consider LB model as an alternative numerical scheme to solve Navier-Stokes equations. Over the past twenty years, LB method has emerged as a competitive scheme for simulating nearly incompressible flows [10]. In order to expend LB method to the simulation of compressible flow, various of compressible LB models have been proposed. In 1993, Alexander et al. [11] and Qian [12] proposed multi-speed (MS) model respectively. Yan et al. [13, 14] constructed a multi-speed and multi-energy-level model. Sun [15, 16], Shi et al. [17], Kataoka et al. [18, 19], and Watari [20] devised several models that introduced an extra energy into the definition of total internal energy. He et al. [21] proposed the first double-distribution-function (DDF) model in 1998. On this basis, Guo et al. [22] and Li et al. [23] developed a total energy DDF model and potential energy DDF model respectively.

LB method was first used to study the wave propagation by Buick et al. [24, 25]. In 2001, Haydock and Yeomans [26] investigated sound-boundary of acoustic streaming for different geometries. Since then, the studies on the application of LB method to acoustics are becoming more and more popular. The accuracy and low-dissipative capability of LB model for acoustic computations were indicated by Marié et al. [27, 28]. Xu and Sagaut [29] proposed a dispersion-relation-preserving LB model to reduce the dispersion and dissipation errors in CAA simulations. Kang et al. [30], Tsutahara et al. [31], Laffite and Pérot [32] simulated the acoustic sounds generated by uniform flow around a circular cylinder. Tamura and Tsutahara [33] calculated the noises caused by blade-vortex interaction using a finite difference LB method. A LB model with a very large eddy simulation approach was used to investigate the noise generated during the interactions between the flow and the rod-airfoil structure [34]. Kusano et al. [5] simulated airfoil self-noise using a multi-scale LB model. So far, most of the applications of LB method to CAA are low Mach number cases. For the higher Mach number flows, the ordinary LB model, which can only handle weakly compressible flows, is not available. In this paper, the potential energy DDF LB model [23] is applied to computationally investigate the aeroacoustic behavior of the transonic flow around a NACA0012 airfoil directly.

The rest of the paper is organized as follows. The compressible LB model and numerical methods are described in Section 2 and Section 3, respectively. Section 4 presents selected numerical simulations including the simulations of the low speed flow around a circular cylinder and the higher speed flows around a NACA0012 airfoil. Finally, some remarks concluded from this study are grouped in Section 5.

https://doi.org/10.4208/aamm.2015.m1083 Published online by Cambridge University Press

2 Compressible LB model

In the potential energy DDF LB model, an extra potential energy distribution function corresponding to the internal freedoms [23] is introduced to overcome the weakness that the adjustable specific-heat ratio and Prandtl number can not be get from a Boltzmann BGK equation. As a result, the governing equations become

$$\frac{\partial f_\alpha}{\partial t}+(\boldsymbol{e}_\alpha\cdot\boldsymbol{\nabla})f_\alpha=-\frac{1}{\tau_f}(f_\alpha-f_\alpha^{eq}), \tag{2.1a}$$

$$\frac{\partial g_\alpha}{\partial t}+(\boldsymbol{e}_\alpha\cdot\boldsymbol{\nabla})g_\alpha=-\frac{1}{\tau_g}(g_\alpha-g_\alpha^{eq})+\frac{Z_\alpha}{\tau_{gf}}(f_\alpha-f_\alpha^{eq}), \tag{2.1b}$$

where the subscripts α denote directions of discrete particle velocity and $\boldsymbol{e}_\alpha$ is the discrete particle velocity vector. f_α is a density distribution function and f_α^{eq} is the corresponding equilibrium distribution function. Similarly, g_α is a potential energy distribution function and g_α^{eq} is the corresponding equilibrium distribution function. Relaxation times of the density distribution function and potential energy distribution function are defined as $\tau_f=\mu/p$ and $\tau_g=\tau_f/\mathrm{Pr}$ respectively, where $p=\rho RT$ is the pressure. τ_{gf} and Z_α can be obtained by

$$\tau_{gf}=\frac{\tau_f\tau_g}{\tau_g-\tau_f},\quad Z_\alpha=\frac{(\boldsymbol{e}_\alpha-\boldsymbol{u})^2}{2}. \tag{2.2}$$

Generally, the dynamic viscosity μ has a relationship with the temperature T and can be estimated from the Sutherland law [35]

$$\mu=\mu_\infty\frac{1+C}{T+C}T^{3/2},\quad C=0.3686, \tag{2.3}$$

where μ_∞ is the freestream dynamic viscosity.

The macroscopic quantities (density, momentums, and total energy) are calculated by

$$\rho=\sum_\alpha f_\alpha,\quad \rho\boldsymbol{u}=\sum_\alpha f_\alpha\boldsymbol{e}_\alpha,\quad \rho E=\frac{b}{2}RT+\frac{1}{2}\rho\boldsymbol{u}^2=\sum_\alpha(f_\alpha\boldsymbol{e}_\alpha^2/2+g_\alpha). \tag{2.4}$$

The D2Q17 (two-dimension-seventeen-velocity, see Fig. 1) lattice based circular distribution function which is proposed by Qu et al. [36] is used as the density distribution function and its specific form can be seen in Appendix B of [23]. The potential energy equilibrium distribution function can be simply obtained from the density distribution function

$$g^{eq}=\frac{b-D}{2}RTf^{eq}, \tag{2.5}$$

where b is the number of degrees of freedom (DOF) and D is the space dimension.

https://doi.org/10.4208/aamm.2015.m1083 Published online by Cambridge University Press

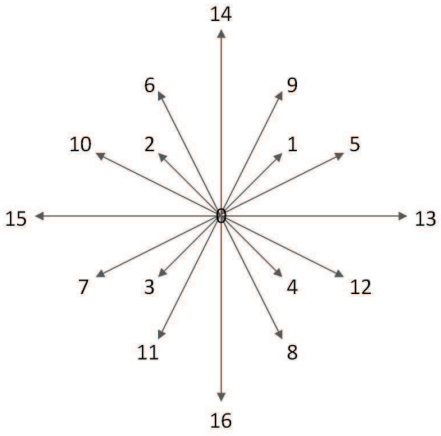


Figure 1: D2Q17 discrete velocity model.

Through the Chapman-Enskog expansion, the compressible Navier-Stokes equations can be recovered

$$\partial_t \rho + \nabla \cdot (\rho \boldsymbol{u}) = 0, \tag{2.6a}$$

$$\partial_t (\rho \boldsymbol{u}) + \nabla \cdot (\rho \boldsymbol{u}\boldsymbol{u}) = -\nabla p + \nabla \cdot \boldsymbol{\tau}, \tag{2.6b}$$

$$\partial_t (\rho E) + \nabla \cdot [(p+\rho E)\boldsymbol{u}] = \nabla \cdot (\lambda \nabla T) + \nabla \cdot (\boldsymbol{\tau} \cdot \boldsymbol{u}), \tag{2.6c}$$

where $\boldsymbol{\tau} = \mu[\boldsymbol{S} - (2/b)(\nabla \cdot \boldsymbol{u})\boldsymbol{I}]$ ($S_{\alpha\beta} = \partial_\alpha u_\beta + \partial_\beta u_\alpha$) is the viscous stress tensor, and $\lambda = [(b+2)/2]R\tau_g p = c_p \tau_g p$ is the thermal conductivity. The specific heat ratio $\gamma = (b+2)/b$.

3 Numerical methods

In compressible LB models, the finite difference (FD) or finite volume (FV) schemes are often used [23, 31, 37, 38]. There are many mature numerical schemes which can be borrowed from the traditional Navier-Stokes equations based methods. In the present study, the convective term is evaluated by the third order Monotone Upwind Scheme for Scalar Conservation Laws (MUSCL) finite volume scheme [39,40] and the second order implicit-explicit (IMEX) Runge-Kutta scheme is applied for the time advancement [37, 41].

Eq. (2.1a) and Eq. (2.1b) can be written as the finite volume form [9, 42]

$$\frac{\partial f_\alpha}{\partial t} + \frac{1}{A}\oint_\Gamma F_\alpha d\Gamma = -\frac{1}{\tau_f}(f_\alpha - f_\alpha^{eq}), \tag{3.1a}$$

$$\frac{\partial g_\alpha}{\partial t} + \frac{1}{A}\oint_\Gamma G_\alpha d\Gamma = -\frac{1}{\tau_g}(g_\alpha - g_\alpha^{eq}) + \frac{Z_\alpha}{\tau_{gf}}(f_\alpha - f_\alpha^{eq}), \tag{3.1b}$$

where A is the area of the cell, Γ is the corresponding cell-boundary, and

$$F_\alpha = (\boldsymbol{e}_\alpha \cdot \boldsymbol{n}) f_\alpha, \quad G_\alpha = (\boldsymbol{e}_\alpha \cdot \boldsymbol{n}) g_\alpha, \tag{3.2}$$

https://doi.org/10.4208/aamm.2015.m1083 Published online by Cambridge University Press

$\boldsymbol{n}$ is the outward-directed unit normal vector.

To advance distribution functions from time t to $t+\Delta t$, the following computations are conducted

$$f_\alpha^{\langle m\rangle}=\frac{f_\alpha^t-\Delta t\sum\limits_{n=1}^{m-1}\tilde{a}_{mn}\left(\frac{1}{A}\oint_\Gamma F_\alpha d\Gamma\right)^{\langle n\rangle}+\Delta t\sum\limits_{n=1}^{m-1}a_{mn}\frac{f_\alpha^{eq\langle n\rangle}-f_\alpha^{\langle n\rangle}}{\tau_f^{\langle n\rangle}}+\frac{\Delta t}{\tau_f^{\langle m\rangle}}a_{mm}f_\alpha^{eq\langle m\rangle}}{1+\frac{\Delta t}{\tau_f^{\langle m\rangle}}a_{mm}}, \tag{3.3a}$$

$$f_\alpha^{t+\Delta t}=f_\alpha^t-\Delta t\sum_{m=1}^{l}\tilde{w}_m\left(\frac{1}{A}\oint_\Gamma F_\alpha d\Gamma\right)^{\langle m\rangle}+\Delta t\sum_{m=1}^{l}w_m\frac{f_\alpha^{eq\langle m\rangle}-f_\alpha^{\langle m\rangle}}{\tau_f^{\langle m\rangle}}, \tag{3.3b}$$

$$g_\alpha^{\langle m\rangle}=\frac{g_\alpha^t-\Delta t\sum\limits_{n=1}^{m-1}\tilde{a}_{mn}\left(\frac{1}{A}\oint_\Gamma G_\alpha d\Gamma\right)^{\langle n\rangle}+\Delta t\sum\limits_{n=1}^{m-1}a_{mn}\frac{g_\alpha^{eq\langle n\rangle}-g_\alpha^{\langle n\rangle}}{\tau_g^{\langle n\rangle}}+\frac{\Delta t}{\tau_g^{\langle m\rangle}}a_{mm}g_\alpha^{eq\langle m\rangle}+\Delta t\sum\limits_{n=1}^{m}a_{mn}Z_\alpha\frac{f_\alpha^{\langle n\rangle}-f_\alpha^{eq\langle n\rangle}}{\tau_{gf}^{\langle n\rangle}}}{1+\frac{\Delta t}{\tau_g^{\langle m\rangle}}a_{mm}}, \tag{3.3c}$$

$$g_\alpha^{t+\Delta t}=g_\alpha^t-\Delta t\sum_{m=1}^{l}\tilde{w}_m\left(\frac{1}{A}\oint_\Gamma G_\alpha d\Gamma\right)^{\langle m\rangle}+\Delta t\sum_{m=1}^{l}w_m\left(\frac{g_\alpha^{eq\langle m\rangle}-g_\alpha^{\langle m\rangle}}{\tau_g^{\langle m\rangle}}+Z_\alpha\frac{f_\alpha^{\langle m\rangle}-f_\alpha^{eq\langle m\rangle}}{\tau_{gf}^{\langle m\rangle}}\right), \tag{3.3d}$$

where

$$\tilde{a}_{mn}=\begin{bmatrix}0&0&0\\0&0&0\\0&1&0\end{bmatrix},\qquad a_{mn}\begin{bmatrix}1/2&0&0\\-1/2&1/2&0\\0&1/2&1/2\end{bmatrix}, \tag{3.4a}$$

$$\tilde{w}_m=\begin{bmatrix}0&1/2&1/2\end{bmatrix},\qquad w_m=\begin{bmatrix}0&1/2&1/2\end{bmatrix}. \tag{3.4b}$$

It is noted that $f_\alpha^{eq\langle m\rangle}$, $g_\alpha^{eq\langle m\rangle}$, and $\tau_f^{\langle m\rangle}$ which related to density, momentums and total energy at m step is unknown. Fortunately, density, momentums and total energy are conservative and can be obtained by

$$\rho^{\langle m\rangle}=\rho^t-\Delta t\sum_{n=1}^{m-1}\left[\tilde{a}_{mn}\sum_\alpha\left(\frac{1}{A}\oint_\Gamma F_\alpha d\Gamma\right)^{\langle n\rangle}\right], \tag{3.5a}$$

$$(\rho u)^{\langle m\rangle}=(\rho u)^t-\Delta t\sum_{n=1}^{m-1}\left[\tilde{a}_{mn}\sum_\alpha\left(\frac{1}{A}\oint_\Gamma F_\alpha d\Gamma e_\alpha\right)^{\langle n\rangle}\right], \tag{3.5b}$$

$$(\rho E)^{\langle m\rangle}=(\rho E)^t-\Delta t\sum_{n=1}^{m-1}\left[\tilde{a}_{mn}\sum_\alpha\left(\frac{1}{A}\oint_\Gamma F_\alpha d\Gamma\frac{e_\alpha^2}{2}+\frac{1}{A}\oint_\Gamma G_\alpha d\Gamma\right)^{\langle n\rangle}\right]. \tag{3.5c}$$

For two dimensional structured grids, the convective terms can be written as

$$\begin{aligned}&\frac{1}{A}\oint_\Gamma H_\alpha d\Gamma\\&=\frac{1}{A}(H_{\alpha,i+1/2,j}l_{i+1/2,j}+H_{\alpha,i-1/2,j}l_{i-1/2,j}+H_{\alpha,i,j+1/2}l_{i,j+1/2}+H_{\alpha,i,j-1/2}l_{i,j-1/2}),\end{aligned} \tag{3.6}$$

https://doi.org/10.4208/aamm.2015.m1083 Published online by Cambridge University Press

where $H_{\alpha,i\pm1/2,j}$ and $H_{\alpha,i,j\pm1/2}$ are numerical fluxes on the interfaces of a cell (i,j), $l_{i\pm1/2,j}$ and $l_{i,j\pm1/2}$ are lengths of the corresponding interface. And

$$H_{\alpha,i+1/2,j}=\begin{cases}(\boldsymbol{e}_\alpha\cdot\boldsymbol{n})h^L_{\alpha,i+1/2,j}, & \boldsymbol{e}_\alpha\cdot\boldsymbol{n}\geq 0,\\ (\boldsymbol{e}_\alpha\cdot\boldsymbol{n})h^R_{\alpha,i+1/2,j}, & \boldsymbol{e}_\alpha\cdot\boldsymbol{n}<0,\end{cases} \tag{3.7}$$

here h denotes both f and g. In MUSCL, the distribution functions on the left and right sides of the interface $(i+1/2,j)$, $h^L_{\alpha,i+1/2,j}$, and $h^R_{\alpha,i+1/2,j}$, are determined as

$$h^L_{\alpha,i+1/2,j}=h_{\alpha,i,j}+\left\{\frac{s}{4}[(1-\kappa s)\Delta_-+(1+\kappa s)\Delta_+]\right\}_i, \tag{3.8a}$$

$$h^R_{\alpha,i+1/2,j}=h_{\alpha,i+1,j}-\left\{\frac{s}{4}[(1-\kappa s)\Delta_++(1+\kappa s)\Delta_-]\right\}_{i+1}, \tag{3.8b}$$

where $\kappa=1/3$ and s is the Van Albada limiter [43]

$$s=\frac{2\Delta_+\Delta_-+\varepsilon^2}{\Delta_+^2+\Delta_-^2+\varepsilon},\quad (\Delta_+)_i=h_{\alpha,i+1,j}-h_{\alpha,i,j},\quad (\Delta_-)_i=h_{\alpha,i,j}-h_{\alpha,i-1,j}. \tag{3.9}$$

ε is a small number to prevent possible division by zero in regions of zero gradient.

On the boundaries of the computational domain, the nonequilibrium extrapolation boundary condition [44] and absorbing boundary condition [45] are used.

The nonequilibrium extrapolation boundary condition is used for the non-slip boundary condition at the wall. This method is of second-order accuracy. Assume that x_b is a boundary node, and x_f is the nearest neighboring fluid node of x_b. Then, the distribution function at x_b is set to be

$$h_\alpha(x_b)=h^{eq}_\alpha(x_b)+[h_\alpha(x_f)-h^{eq}_\alpha(x_f)]. \tag{3.10}$$

The absorbing boundary condition consists in using a buffer between the fluid region and the open boundary to create an asymptotic transition towards a target flow defined in terms of target distribution functions. This is done by adding an extra term to governing equations. Take the density distribution function for example, Eq. (2.1a) becomes

$$\frac{\partial f_\alpha}{\partial t}+(e_\alpha\cdot\nabla)f_\alpha=-\frac{1}{\tau_f}(f_\alpha-f^{eq}_\alpha)-\sigma(f^{eq}_\alpha-f^T_\alpha), \tag{3.11}$$

where $\sigma=\sigma_m(\delta/d)^2$ is the absorption coefficient, σ_m is a constant, δ is the distance measured from the beginning of the buffer zone and d is the width of the buffer. f^T_α is the target density distribution function and keeps as initial value all the time.

4 Numerical simulations

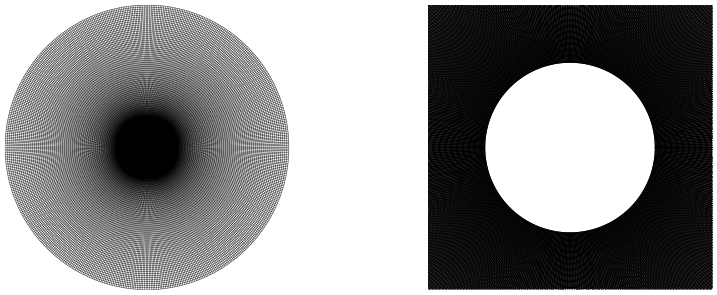
For the flows around a circular cylinder, the simulations are characterized by the Reynolds number $Re=\rho_\infty u_\infty L/\mu_\infty$ and the Mach number $M=u_\infty/c_s$, where $c_s=\sqrt{\gamma RT_\infty}$ is the

https://doi.org/10.4208/aamm.2015.m1083 Published online by Cambridge University Press

sound speed. For the flows around a airfoil, there is another parameter, the angle of attack α. In this section, the flow around a circular cylinder at Re=150, M=0.2 is simulated firstly. Then flows around a NACA0012 airfoil at Re=5000, M=0.5, α=0° and Re=10000, $M=0.8$, $\alpha=0°$ are simulated respectively. Throughout this section, the reference quantities (ρ_{ref}, u_{ref}, and T_{ref}) are all set to 1.0. The specific-heat ratio is 1.4, and the Prandtl number is 0.71.

4.1 Flow around a circular cylinder

The flow around a circular cylinder at low Mach number is an important benchmark of aeroacoustic simulation to study the generation and propagation mechanisms of sound [32, 46, 47]. Here laminar vortex shedding from a circular cylinder at $Re=150$ and $M=0.2$ is considered. The diameter is chosen as characteristic length L and viewed as 1. An O-grid (see Fig. 2) is applied and the grid size is 503×871 in wall-azimuthal and normal directions. The height of the first layer grid is 5×10^{-3}. The outer ten nodes in wall-normal direction are buffer nodes. The outermost nodes keep the equilibria of initial state. At the body surface, no-slip boundary condition are imposed. In this case, the time step is $\Delta t=2\times10^{-3}$.



(a) Far field (b) Near field

Figure 2: O-type grid.

Fig. 3 and Fig. 4 show the instantaneous pressure field and the vortex field in the vicinity of the circular cylinder respectively. It is clearly seen that vortexes shed from the circular cylinder to the wake. As a result of the vortex shedding, the circular cylinder experiences oscillating drag coefficient $C_D=F_d/(\frac{1}{2}\rho_\infty u_\infty^2 L)$ and lift coefficient $C_L=F_l/(\frac{1}{2}\rho_\infty u_\infty^2 L)$ (see Fig. 5). Fig. 6 shows the time-averaged pressure coefficient $Cp_{ave}=(p_{ave}-p_\infty)/(\frac{1}{2}\rho_\infty u_\infty^2 L)$ distribution on the surface of the circular cylinder, where p_{ave} is time-averaged pressure. The pressure coefficient obtained in this study looks in very good agreement with the simulation result as reported in [46]. Fig. 7 shows the instantaneous distribution of the acoustic pressure $\Delta p=p-p_{ave}$. The white part is high pressure region and the black part is low pressure region. Due to the Doppler effect, the

https://doi.org/10.4208/aamm.2015.m1083 Published online by Cambridge University Press

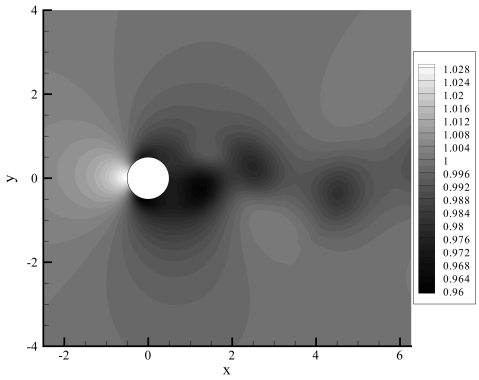


Figure 3: Instantaneous pressure field in the vicinity of the circular cylinder.

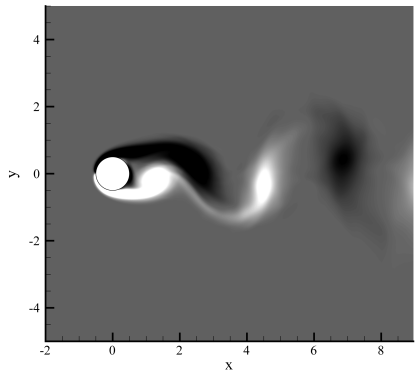


Figure 4: Instantaneous vortex field in the vicinity of the circular cylinder.

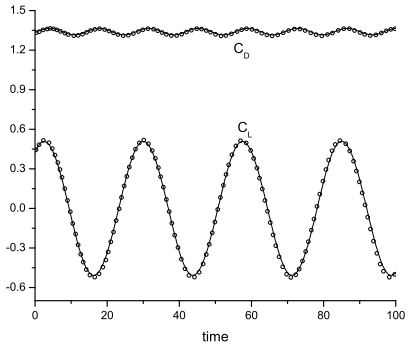


Figure 5: Lift coefficient and drag coefficient of flow around the circular cylinder. The circles are for present results and solid lines are for Inoue's results.

pressure fluctuation on the upstream side is more dense than that on the downstream side.

https://doi.org/10.4208/aamm.2015.m1083 Published online by Cambridge University Press

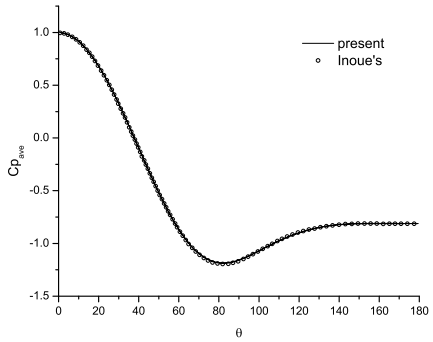


Figure 6: Time-averaged pressure coefficient around the circular cylinder.

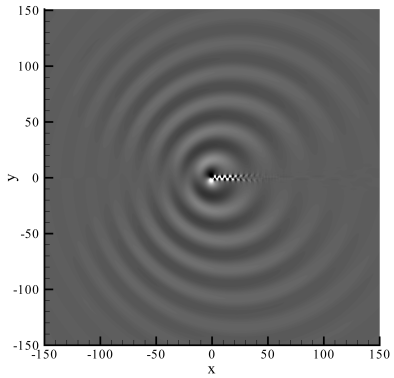


Figure 7: Acoustic pressure field of flow around the circular cylinder.

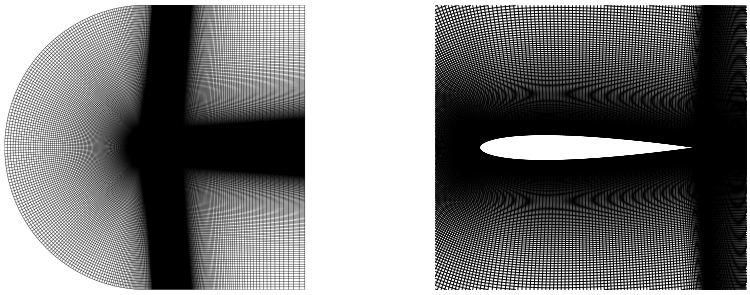
4.2 Flows around a NACA0012 airfoil

To simulate the flows around a NACA0012 airfoil, a C-type grid (see Fig. 8) with grid resolution of 1501×401 is used. There are 301 points on the surface of airfoil and the height of the first layer grid is 2.5×10^{-4}. The time step is $\Delta t=1.25\times10^{-4}$. The chord is chosen as characteristic length L and viewed as 1. At the body surface, no-slip condition for velocity and adiabatic wall condition for temperature are imposed. A periodic boundary condition is applied at the grid-cut in the wake. Similar with the previous subsection, the outermost nodes keep the equilibria of initial state and the next ten nodes are buffer nodes.

In order to validate the code of compressible LB model, we first simulated a steady state at $Re=5000$, $M=0.5$, $\alpha=0^\circ$. Fig. 9 groups pressure field in the vicinity of the airfoil. The lift coefficient is almost zero 4×10^{-13} and the drag coefficient is equal to 0.0565 which is very close to the value 0.0561 in [48]. The wall pressure coefficients are presented in Fig. 10. It is seen that our results are nearly coincide with the results of Bassi [49].

For the direct simulation of flow around the NACA0012 airfoil at $Re=10000$, $M=0.8$,

https://doi.org/10.4208/aamm.2015.m1083 Published online by Cambridge University Press



(a) Far field (b) Near field

Figure 8: C-type grid.

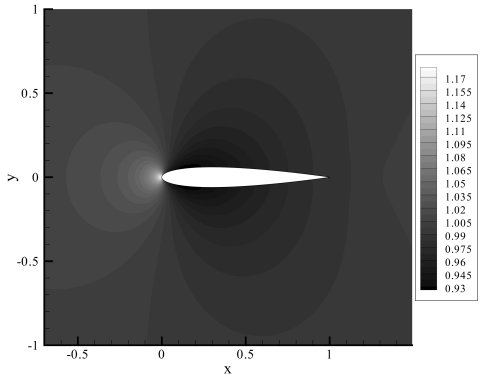


Figure 9: Pressure field in the vicinity of the airfoil ($Re=5000$, $M=0.5$, $\alpha=0^\circ$).

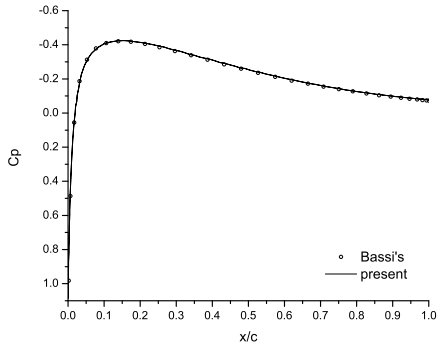


Figure 10: Pressure coefficient around the airfoil ($Re=5000$, $M=0.5$, $\alpha=0^\circ$).

$\alpha=0^\circ$, Bouhadji [50] and Jones [35] had investigated the fluctuating flow field. But their results are totally different. Bouhadji found that the flow fluctuated with two frequencies. In Jones's results, there was only one frequency. At present, Fig. 11 and Fig. 12 are the

https://doi.org/10.4208/aamm.2015.m1083 Published online by Cambridge University Press

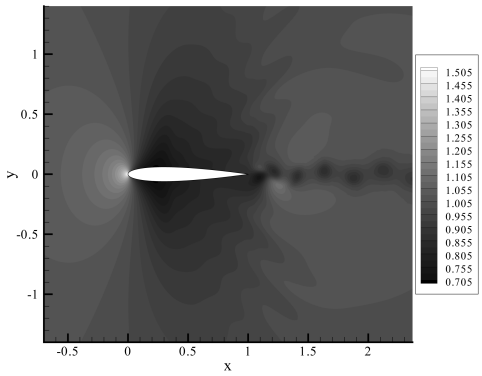


Figure 11: Instantaneous pressure field in the vicinity of the airfoil ($Re=10000$, $M=0.8$, $\alpha=0^\circ$).

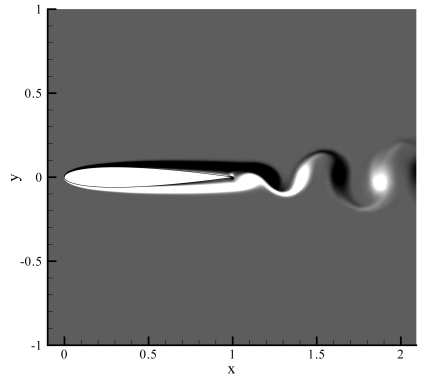


Figure 12: Instantaneous vortex field in the vicinity of the airfoil ($Re=10000$, $M=0.8$, $\alpha=0^\circ$).

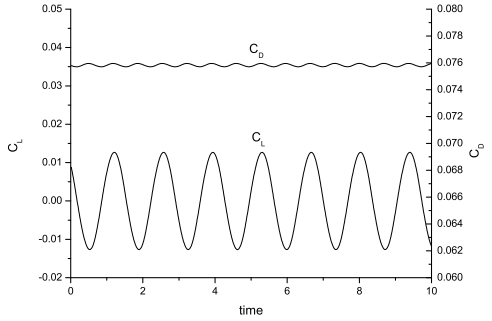


Figure 13: Lift coefficient and drag coefficient of flow around the airfoil ($Re=10000$, $M=0.8$, $\alpha=0^\circ$).

instantaneous pressure field and vortex field respectively. In Fig. 11, there are obviously fluctuations not only in the wake but also above and below the airfoil. The time histories of lift coefficient and drag coefficient are illustrated in Fig. 13. It can be seen that there

https://doi.org/10.4208/aamm.2015.m1083 Published online by Cambridge University Press

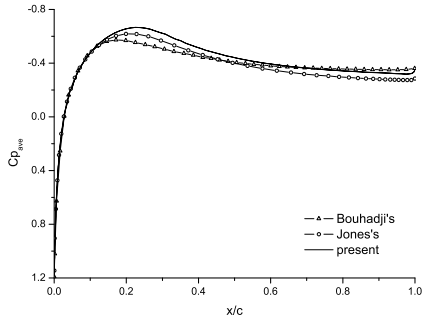


Figure 14: Time-averaged pressure coefficient around the airfoil ($Re=10000$, $M=0.8$, $\alpha=0^\circ$).

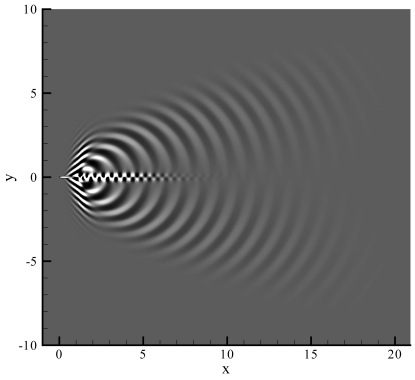


Figure 15: Acoustic pressure field of flow around the airfoil ($Re=10000$, $M=0.8$, $\alpha=0^\circ$).

is only one frequency in our result. Fig. 14 shows the time-averaged pressure coefficient distribution on the surface of the airfoil. Our curve has the same trend with that of Jones but our result is higher. The instantaneous sound pressure field is plotted in Fig. 15. Because of the existence of the supersonic flow region, the forward propagation pressure fluctuation decays very fast and is suppressed to the middle part of the airfoil. But the forward propagation pressure fluctuation is so large that it can affect the pressure field as shown in Fig. 11. By contrast, the backward propagation pressure fluctuation is a little weaker. But its propagation is far more and has obvious directivity.

5 Conclusions

In this paper, direct numerical simulations of two-dimension laminar flows around a circular cylinder at $Re=150$, $M=0.2$ and around a NACA0012 airfoil at $Re=10000$, $M=0.8$, $\alpha=0^\circ$ are performed based on the potential energy double-distribution-function lattice Boltzmann method. Meanwhile, the aeroacoustic characteristics of the whole domain are also obtained. For computational method, the MUSCL finite volume scheme and IMEX

https://doi.org/10.4208/aamm.2015.m1083 Published online by Cambridge University Press

Runge-Kutta scheme are used on body-fitted grids. Through the comparison, the results of flow around a circular cylinder agree well with the reference results. To validate our code for the simulation of compressible flow, a steady flow around a NACA0012 airfoil at $Re=5000$, $M=0.5$, $\alpha=0^\circ$ is tested and a good agreement is obtained. For the unsteady flow around a NACA0012 airfoil, a one frequency fluctuated flow which is similar with the result of Jones is obtained. It is found that the forward propagation pressure fluctuation is strong but decays fast and the backward propagation pressure fluctuation is weak but decays slowly. Moreover, the backward propagation pressure fluctuation has obvious directivity.

Acknowledgments

This project was financially supported mainly by the Innovation Fund for Aerospace Science and Technology of China (Grant No. 2009200066), the National Pre-Research Foundation of China (Grant No. 9140A13040111HK0329) and the Aeronautical Science Fund of China (Grant No. 20111453012).

References

[1] X. Li, R. K. Leung and R. C. So, *One-step aeroacoustics simulation using lattice Boltzmann method,* AIAA J., 44 (2006), pp. 78–89.
[2] E. M. Viggen, *Viscously damped acoustic waves with the lattice Boltzmann method,* Philos. T. Roy. Soc. A, 369 (2011), pp. 2246–2254.
[3] S. Tajiri, M. Tsutahara and H. Tanaka, *Direct simulation of sound and underwater sound generated by a water drop hitting a water surface using the finite difference lattice Boltzmann method,* Comput. Math. Appl., 59 (2010), pp. 2411–2420.
[4] T. Ikeda, T. Atobe and S. Takagi, *Direct simulations of trailing-edge noise generation from two-dimensional airfoils at low Reynolds numbers,* J. Sound Vibration, 331 (2012), pp. 556–574.
[5] K. Kusano, K. Yamada and M. Furukawa, *Toward direct numerical simulation of aeroacoustic field around airfoil using multi-scale lattice Boltzmann method*, ASME 2013 Fluids Engineering Division Summer Meeting, American Society of Mechanical Engineers, Nevada, USA, 2013, V01AT09A005.
[6] A. Xu, G. Zhang, Y. Li and H. Li, *Modeling and simulation of nonequilibrium and multiphase complex systems: lattice Boltzmann kinetic theory and application,* Progress Phys., 34 (2014), pp. 136–167, in Chinese.
[7] A. Xu, C. Lin, G. Zhang and Y. Li, *Multiple-relaxation-time lattice Boltzmann kinetic model for combustion,* Phys. Rev. E, 91 (2015), 043306.
[8] P. L. Bhatnagar, E. P. Gross and M. Krook, *A model for collision processes in gases i. small amplitude processes in charged and neutral one-component systems*, Phys. Rev., 94 (1954), pp. 511–525.
[9] S. Succi, The Lattice Boltzmann Equation: for Fluid Dynamics and Beyond, Oxford University Press, 2001.
[10] A. G. Xu, G. C. Zhang, Y. B. Gan, F. Chen and X. J. Yu, *Lattice Boltzmann modeling and simulation of compressible flows,* Frontiers Phys., 7 (2012), pp. 582–600.

https://doi.org/10.4208/aamm.2015.m1083 Published online by Cambridge University Press

[11] F. J. ALEXANDER, S. CHEN AND J. D. STERLING, *Lattice Boltzmann thermohydrodynamics,* Phys. Rev. E, 47 (1993), pp. R2249–R2252.
[12] Y. QIAN, *Simulating thermohydrodynamics with lattice BGK models*, J. Sci. Comput., 8 (1993), pp. 231–242.
[13] G. YAN, Y. CHEN AND S. HU, *Simple lattice Boltzmann model for simulating flows with shock wave,* Phys. Rev. E, 59 (1999), pp. 454–459.
[14] G. YAN, J. ZHANG, Y. LIU AND Y. DONG, *A multi-energy-level lattice Boltzmann model for the compressible Navier-Stokes equations,* Int. J. Numer. Methods Fluids, 55 (2007), pp. 41–56.
[15] C. SUN, *Lattice-Boltzmann models for high speed flows,* Phys. Rev. E, 58 (1998), pp. 7283–7287.
[16] C. SUN, *Adaptive lattice Boltzmann model for compressible flows: viscous and conductive properties,* Phys. Rev. E, 61 (2000), pp. 2645–2653.
[17] W. SHI, W. SHYY AND R. MEI, *Finite-difference-based lattice Boltzmann method for inviscid compressible flows,* Numer. Heat Transfer B Fundamentals, 40 (2001), pp. 1–21.
[18] T. KATAOKA AND M. TSUTAHARA, *Lattice Boltzmann model for the compressible Euler equations,* Phys. Rev. E, 69 (2004), 056702.
[19] T. KATAOKA AND M. TSUTAHARA, *Lattice Boltzmann model for the compressible Navier-Stokes equations with flexible specific-heat ratio,* Phys. Rev. E, 69 (2004), 035701.
[20] M. WATARI, *Finite difference lattice Boltzmann method with arbitrary specific heat ratio applicable to supersonic flow simulations,* Phys. A Stat. Mech. Appl., 382 (2007), pp. 502–522.
[21] X. HE, S. CHEN AND G. D. DOOLEN, *A novel thermal model for the lattice Boltzmann method in incompressible limit*, J. Comput. Phys., 146 (1998), pp. 282–300.
[22] Z. GUO, C. ZHENG, B. SHI AND T. S. ZHAO, *Thermal lattice Boltzmann equation for low Mach number flows: decoupling model,* Phys. Rev. E, 75 (2007), 036704.
[23] K. LI AND C. ZHONG, *A lattice Boltzmann model for simulation of compressible flows,* Int. J. Numer. Methods Fluids, 77 (2015), pp. 334–357.
[24] J. BUICK, C. GREATED AND D. CAMPBELL, *Lattice BGK simulation of sound waves,* Europhys. Lett., 43 (1998), pp. 235–240.
[25] J. BUICK, C. BUCKLEY, C. GREATED AND J. GILBERT, *Lattice Boltzmann BGK simulation of nonlinear sound waves: the development of a shock front*, J. Phys. A Math. General, 33 (2000), pp. 3917–3928.
[26] D. HAYDOCK AND J. YEOMANS, *Lattice Boltzmann simulations of acoustic streaming,* J. Phys. A Math. General, 34 (2001), pp. 5201–5213.
[27] S. MARIÉ, D. RICOT AND P. SAGAUT, *Accuracy of lattice Boltzmann method for aeroacoustics simulations,* AIAA Paper, 3515 (2007).
[28] S. MARIÉ, D. RICOT AND P. SAGAUT, *Comparison between lattice Boltzmann method and Navier-Stokes high order schemes for computational aeroacoustics,* J. Comput. Phys., 228 (2009), pp. 1056–1070.
[29] H. XU AND P. SAGAUT, *Optimal low-dispersion low-dissipation LBM schemes for computational aeroacoustics*, J. Comput. Phys., 230 (2011), pp. 5353–5382.
[30] H. K. KANG, K. D. RO, M. TSUTAHARA AND Y. H. LEE, *Numerical prediction of acoustic sounds occurring by the flow around a circular cylinder,* KSME Int. J., 17 (2003), pp. 1219–1225.
[31] M. TSUTAHARA, T. KONDO AND K. MOCHIZUKI, *Direct simulations of acoustic waves by finite volume lattice Boltzmann method,* AIAA Paper, 2570 (2006).
[32] A. LAFFITE AND F. PÉROT, *Investigation of the noise generated by cylinder flows using a direct lattice-Boltzmann approach,* AIAA Paper, 3268 (2009).
[33] A. TAMURA, M. TSUTAHARA, T. KATAOKA, T. AOYAMA AND C. YANG, *Numerical simulation of two-dimensional blade-vortex interactions using the finite difference lattice Boltzmann*

https://doi.org/10.4208/aamm.2015.m1083 Published online by Cambridge University Press

method, AIAA J., 46 (2008), pp. 2235–2247.
[34] R. SATTI, P. T. LEW, Y. LI, R. SHOCK AND S. NOELTING, *Unsteady flow computations and noise predictions on a rod-airfoil using lattice Boltzmann method,* AIAA Paper, 497 (2009).
[35] L. E. JONES, Numerical Studies of the Flow Around an Airfoil at Low Reynolds Number, PhD thesis, University of Southampton, 2008.
[36] K. Qu, Development of Lattice Boltzmann Method for Compressible Flows, PhD thesis, National University of Singapore, 2009.
[37] Q. LI, Y. L. HE, Y. WANG AND W. Q. TAO, *Coupled double-distribution-function lattice Boltzmann method for the compressible Navier-Stokes equations,* Phys. Rev. E, 76 (2007), 056705.
[38] M. TSUTAHARA, *The finite-difference lattice Boltzmann method and its application in computational aero-acoustics,* Fluid Dyn. Research, 44 (2012), 045507.
[39] B. VAN LEER, *Towards the ultimate conservative difference scheme. v. a second-order sequel to godunov's method*, J. Comput. Phys., 32 (1979), pp. 101–136.
[40] M. KERMANI, A. GERBER AND J. STOCKIE, *Thermodynamically based moisture prediction using Roe's scheme,* 4th Conference of Iranian Aerospace Society, Amir Kabir University of Technology, Tehran, Iran, 2003, pp. 27–29.
[41] L. PARESCHI AND G. RUSSO, *Implicit-explicit Runge-Kutta schemes and applications to hyperbolic systems with relaxation,* J. Sci. Comput., 25 (2005), pp. 129–155.
[42] D. PATIL, *Chapman-Enskog analysis for finite-volume formulation of lattice Boltzmann equation*, Phys. A Stat. Mech. Appl., 392 (2013), pp. 2701–2712.
[43] G. VAN ALBADA, B. VAN LEER AND W. ROBERTS JR, *A comparative study of computational methods in cosmic gas dynamics,* Astronomy Astrophys., 108 (1982), pp. 76–84.
[44] Z. GUO, C. ZHENG AND B. SHI, *Non-equilibrium extrapolation method for velocity and pressure boundary conditions in the lattice Boltzmann method,* Chinese Phys., 11 (2002), pp. 366–374.
[45] A. R. DA SILVA, Numerical Studies of Aeroacoustic Aspects of Wind Instruments, PhD thesis, McGill University, 2008.
[46] O. INOUE AND N. HATAKEYAMA, *Sound generation by a two-dimensional circular cylinder in a uniform flow,* J. Fluid Mech., 471 (2002), pp. 285–314.
[47] M. TSUTAHARA, T. KATAOKA, K. SHIKATA AND N. TAKADA, *New model and scheme for compressible fluids of the finite difference lattice Boltzmann method and direct simulations of aerodynamic sound,* Comput. Fluids, 37 (2008), pp. 79–89.
[48] D. J. MAVRIPLIS AND A. JAMESON, *Multigrid solution of the Navier-Stokes equations on triangular meshes,* AIAA J., 28 (1990), pp. 1415–1425.
[49] F. BASSI AND S. REBAY, *A high-order accurate discontinuous finite element method for the numerical solution of the compressible Navier-Stokes equations,* J. Comput. Phys., 131 (1997), pp. 267–279.
[50] A. BOUHADJI AND M. BRAZA, *Organised modes and shock-vortex interaction in unsteady viscous transonic flows around an aerofoil: part i: Mach number effect,* Comput. Fluids, 32 (2003), pp. 1233–1260.

https://doi.org/10.4208/aamm.2015.m1083 Published online by Cambridge University Press